



# Influence of urban land cover data uncertainties on the numerical simulations of urbanization effects in the 2013 high-temperature episode in Eastern China

Ning Zhang<sup>1,2</sup> · Yan Chen<sup>3</sup> · Hao Gao<sup>4</sup> · Ling Luo<sup>5</sup>

Received: 4 December 2018 / Accepted: 17 June 2019 / Published online: 1 July 2019  
© The Author(s) 2019

## Abstract

Updating the urban land cover information has been proved a necessary method for the numerical studies of urban climate and urban atmospheric environment in China, a fast urbanizing country. However, there are uncertainties in the urban land use/cover (ULUC) information in different datasets due to the uncertainties in raw data sources and produce methods. In this study, the Weather Research and Forecasting model is used to simulate the summer climate over the Yangtze River Delta in July and August 2013, when a heatwave episode occurred. Five numerical experiments are designed; one is the baseline experiment (non-urban land cover (NOURB)) in which all urban land covers are removed, and different urban land use/cover (ULUC) experiments from four different global land cover datasets are used in other four experiments. The differences between the ULUC experiments and the NOURB experiment are used to observe the urbanization effects. The results show a remarkable urbanization effect in all the ULUC experiments, and the urbanization influences are most different over the *union-urban* area, which defined as the area marked as urban area by at least one land cover dataset, because the uncertainties in urban land cover information are greatest in this area. All the ULUC experiments show the regional influence of urbanization as well, which means urbanization effects are not limited in cities. The Climate Change Initiative (CCI) experiment using the European Space Agency CCI 2013 dataset showed the greatest urbanization influence and the highest effect index in all analyzed variables, because of the largest urban land cover area in the analysis domain. The urban land cover area in the Global Land Cover experiment is the smallest among the ULUC experiments, but it distributes in a more concentrated way than in other experiments; it indicates that both city size and city shape affect the regional influence.

**Keywords** Urban warming · Numerical modeling · Land use/land cover · Weather research and forecast model · Urbanization effect

✉ Ning Zhang  
ningzhang@nju.edu.cn

<sup>1</sup> CMA-NJU Joint Laboratory for Climate Prediction Studies, Institute for Climate and Global Change Research, School of Atmospheric Sciences, Nanjing University, 163 Xianlin Avenue, Nanjing 210023, China

<sup>2</sup> Jiangsu Collaborative Innovation Center for Climate Change, Nanjing 210093, China

<sup>3</sup> Jiangsu Climate Center, Nanjing 210002, China

<sup>4</sup> National Satellite Meteorological Center of China Meteorological Administration, Beijing 100084, China

<sup>5</sup> Zhejiang Province Meteorological Observatory, Hangzhou 310004, China

## 1 Introduction

In the past decades, China has experienced a very fast urbanization process with the rapid economic development (Xiao et al. 2014). The urban area had tripled and the urban population had doubled in recent decades (Schneider and Mertes 2014), and the process is still undergoing. Urbanization processes modify local and regional climate conditions. One of the most important urban effects is urban warming; the air temperature in cities is usually higher than that in the surrounding sub-urban or rural area, which is named urban heat island (UHI). Strong urban warming effect on climate in China has been found using observations and reanalysis data (Zhou et al. 2004) and satellite observations (Li et al. 2013; Zhao et al. 2014; Zhao and Wu 2017). The reasons of urban

warming are complex, but the changing in underlying surface features is an important cause (Taha 1997). During the urban expansions, the vegetation land covers are replaced by impervious construction materials, which are of higher conductivities and higher heat capacities, and shed water more rapidly; at the same time, the city buildings have more vertical surfaces and form the so-called “urban canopy layer” (Grimmond 2007). These changes modify the physical, radiation, and hydraulic properties of the land surface, then cause the differences of the meteorological environment between urban and non-urban areas (Arnfield 2003). With the development of numerical models, especially the urban canopy models (UCMs), which describe the energy and water exchange between the urban land surface and the atmosphere in a sophisticated way (Chen et al. 2011; Grimmond et al. 2010, 2011); mesoscale numerical models are widely used to evaluate the local or regional impacts of urbanization-induced land use/cover change (LUCC) on urban climate and atmospheric environment. Previous numerical modeling investigations showed that the urbanization-induced LUCC can modify local boundary layer structure (Zhang et al. 2011; Kusaka et al. 2012; Nehrkorn et al. 2013; Kang et al. 2014), regional climate (Zhang et al. 2010, 2016; Thatcher and Hurley 2012; Wang et al. 2013; Li et al. 2014a, b; Zhao and Wu 2017), and urban air quality (Taha 2008; Wang et al. 2009; Lee et al. 2011; Klein et al. 2014).

The Weather Research and Forecasting (WRF; <https://www.mmm.ucar.edu/weather-research-and-forecasting-model>) is a state-of-the-art numerical model and widely used in the numerical studies related to urbanization processes in China due to the sophisticated urban canopy models deployed in it (Chen et al. 2011; Kusaka et al. 2012). The urban land use/cover (ULUC) dataset is important because it supplies the fundamental information to the urban canopy models. The ULUC information is usually a part of the static land cover dataset in the model release stated using an integer index as the other land cover/vegetation cover information. In the early release versions of the WRF, the model used the 24-category U.S. Geological Survey (USGS) global 1-km land cover map, which is derived from the monthly Advanced Very High Resolution Radiometer (AVHRR)–normalized difference vegetation index (NDVI) observations from April 1992 to March 1993 (Loveland et al. 2000). After WRF v3.6, a 15-arc resolution climatological Moderate Resolution Imaging Spectroradiometer (MODIS) land cover set based on the 2001–2010 observation is available (Broxton et al. 2014) and is set as the default database after the WRF v3.8 release. Even several datasets are available in the WRF release; they are not suitable to represent the quick urban expansion processes in the recent decades in China. Previous studies have proved that updated ULUC information will improve the model performance (e.g., Wang et al. 2014, 2016; Zhang et al. 2016; Li et al. 2014a, b). A widely used method is using

the standard dataset of AVHRR or MODIS in the WRF release for the non-urban area and updating the ULUC information (the domain urban classification and the urban cover fractions) with additional sources, such as the annual MODIS datasets (Li et al. 2014a, b; Wang et al. 2013; Zhang et al. 2010; Zhang et al. 2016) and the Landsat data (Yu and Liu 2015; Zhang et al. 2009; Zhang and Chen 2014; Zhang et al. 2011). Other global land cover datasets such as the Global Land Cover-SHARE (GLC-SHARE), GlobCover ([http://due.esrin.esa.int/page\\_globcover.php](http://due.esrin.esa.int/page_globcover.php)), and European Space Agency Climate Change Initiative (ESA CCI) land cover (<https://www.esa-landcover-cci.org/>) are also used in the analysis of urbanization impacts (Ajaaj et al. 2017; Arsanjani et al. 2016; Zhou et al. 2015).

Even the releases of several global land use/land cover datasets enrich the user’s choice, and the updating of the static urban land cover information in the WRF model can improve the model performance (Li et al. 2014a, b); most datasets failed to represent the quick urbanization processes in China because of the data resolution, the classification method, or the training database (Yang et al. 2017). The urban classification in China is more difficult because of the limit of training and validation data (Yang et al. 2013). Most recent works prefer to update the urban land cover information with one specific dataset (such as MODIS, Landsat) due to the limit of available datasets, and little investigations have been carried out to study how different datasets will affect the simulation results. In this study, we used the WRF model as a numerical tool to investigate the impact of the selection of ULUC information from the different global land cover datasets in numerical modeling simulations and the different urbanization effects introduced by such uncertainties.

## 2 Model descriptions and numerical experiment design

The WRF model (version 3.9.1) is used as the numerical tool in this study. The model configuration consists of a parent domain and a nesting domain centered at 120.4 W, 30.6 N, as shown in Fig. 1; the horizontal resolution of the outer domain is 15 km, and that of the inner domain is 3 km. The vertical grid system has 53 levels, and the model top is at 50 hPa. Initial and boundary conditions of models were provided by NCEP FNL data, with a horizontal resolution of 1° and a temporal resolution of 6 h. The Noah land surface model (LSM) was used to calculate the land surface processes including the exchanges of energy and moist between the land surface and the atmosphere. The parameterization schemes used in this study are listed in Table 1. The single-layer urban canopy model (Chen et al. 2011) is deployed to represent the impact of buildings on the radiation transportation, turbulent heat fluxes, and energy exchanges in urban canyons. The

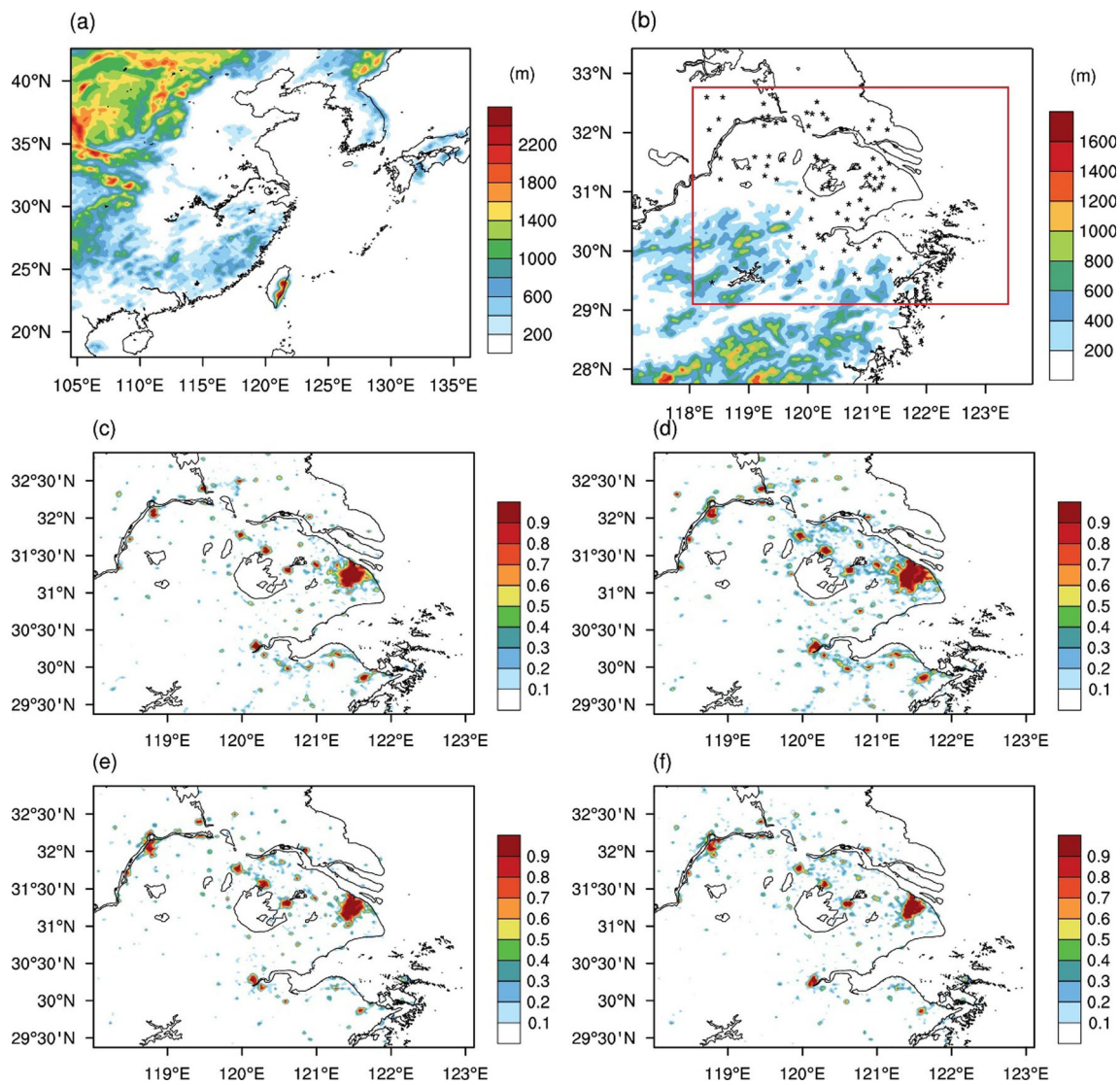


**Fig. 1** The topography of **a** domain 1 and **b** domain 2 and the urban land cover fraction calculated from **c** MODIS, **d** ESA, **e** GLC, and **f** GLO for the analysis area (red line box and the stars in **a** indicate the locations of the observations sites)

other physics packages used in the simulations include the Rapid Radiative Transfer Model for GCMs (RRTM-G) for the longwave radiation, the Goddard scheme for the shortwave radiation processes, and the Mellor-Yamada-Janjic scheme for the planetary boundary layer parameterization.

Four ULUC experiments are designed to study the influence of urban land covers, as shown in Table 2. In each experiment, the default MODIS land use/land cover data in the WRF release were used to represent the current land use/land cover conditions and the urban cover fraction and

**Table 1** Urban area and fraction estimated from the different experiments and analysis areas

Experiment name	Dataset description	Area (km <sup>2</sup> )	Fraction (%)
MOD	500-m-resolution MODIS land cover data of 2013	5229.3	4.6
CCI	300-m-resolution ESA CCI land cover data of 2013	7947.8	7.1
GLC	500-m-resolution Global Land Cover-SHARE of 2010s	3874.6	3.4
GLO	500-m-resolution GlobCover of 2009	4009.2	3.5
Con-urban	The overlaid urban area in 4 datasets	1820.6	1.8
Union-urban	The union of urban area in 4 datasets	9837.5	8.7
NOURB	—	0.0	0.0

**Table 2** Physical process parameterization schemes used in the numerical experiments

Physical process	Parameterization scheme
PBL scheme	Mellor-Yamada-Janjic TKE scheme
Surface layer	Monin-Obukhov (Janjic) scheme
Land surface model	Unified Noah land surface model (with the single-layer urban canopy model)
Microphysics	WSM 6-class Graupel scheme (only used for domain 02)
Shortwave radiation	Dudhia scheme
Longwave radiation	RRTM scheme
Cumulus parameterization	Kain-Fritsch scheme (only used for domain 01)

urban land cover type of each grid were estimated and updated with different land cover databases: the 500-m-resolution MODIS land cover data of 2013 (Land Cover Type Yearly L3 Global 500 m, MCD12Q1) was used for the MOD experiment, the 300-m-resolution ESA CCI land cover data of 2013 was used for the CCI experiment, the 500-m-resolution Global Land Cover (GLC) data was used for the GLC experiment, and the ESA GlobCover data was used for the GLO experiment. At the first stage, the urban land cover fraction of each grid was calculated with different ULUC datasets, then the urban land cover type of each grid was classified into three types based on the urban land cover fraction: for the commercial type, the urban land cover fraction is greater than 90%; for the medium-intensity type, the urban land cover fraction is between 50 and 90%; and for the low-intensity type, the urban land cover fraction is less than 50%. The default urban canopy physical parameters in the WRF release were used for the three urban types due to the lack of detailed urban buildings and fabric data. It should be noticed that this may introduce new uncertainties in the simulations, because the differences in simulations may be caused not only by the ULUC information (the urban land cover fraction) but also by the differences in urban canopy parameters among different urban land cover types. Because the thermal and radiation parameters are the same for all the three urban land cover types in the default WRF release, most of the uncertainties are caused by the urban canyon aspect ratios controlled by the building heights and road widths which are different in different urban land cover types. It has been found in previous studies that the influences of urban canyon aspect are much less than these of the thermal and radiation parameters, such as albedos of urban facets, in the single-layer UCM (Zhao et al. 2014), so the uncertainties caused by the urban canopy physical parameters are taken as a part of the uncertainties caused by urban land cover information in this paper. To investigate the impacts on urban warming effect simulations, a non-urban land cover (NOURB) experiment is designed based on the ULUC experiments with the urban land cover replaced by cropland as in previous studies (Zhang et al. 2010, 2016). This study focuses on the uncertainties

caused by the urban cover information as documented by Xu et al. (2017), so the anthropogenic heat release is excluded in the simulations, and even previous studies have documented its importance (Zhang and Chen 2014; Zhang et al. 2016). The NOURB experiment is designed as a baseline experiment to estimate the urban land cover expanding influences, in which all urban grids were replaced by cropland as in previous studies (Zhang and Chen 2014; Zhang et al. 2010, 2016).

A 2-month high-temperature episode, July and August 2013, is selected as the study period. In the selected period, a month-long heatwave episode took place in the Yangtze River Delta due to the anomalies of the West Pacific subtropical high-pressure system (Chen and Zhang 2018; Wang et al. 2014), in which the air temperature was much higher and the rainfall was dramatically less than the climate mean. Urban heat island occurs more frequently under such synoptic background (Arnfield 2003; Grimmond 2007), and previous studies have proved that the local urban warming also contributed to the heatwave episode in this area (Chen and Zhang 2018; Wang et al. 2016; Zhang and Chen 2014). The model integrations were conducted from 0000 UTC 20 June (0800 LST 20 May) to 0000 UTC 1 September 2013, and the first 10 days (20–30 June) was set as a spin-up period and the results of the whole July and August were analyzed in this study.

The urban warming impact not only changes the microclimate over urban areas; previous studies showed that urbanization leads to regional impacts on surface meteorological fields and precipitation processes. Several studies have tried to quantify the regional impacts using effect indexes (Trusilova et al. 2008; Zhang et al. 2010). The method of Zhang et al. (2010) was used to observe the regional urban impacts in different experiments, in which the effect index (EI) of urbanization is defined as follows:

$$EI(x) = \frac{A_{\text{change}}(x)}{A_{\text{urban}}}$$

where  $x$  can be any meteorological variable, etc.  $A_{\text{change}}(x)$  is the sum of the areas where  $x$  changed in the sensitivity experiments compared to the NOURB experiment, and  $A_{\text{urban}}$  is the sum of the areas of urban grids. If EI is greater than 1, the urbanization-induced LUCC has a regional impact.

To investigate the local impacts of ULUC information difference, three urban area types are defined in this study. The *own-urban* area means the urban area defined by each dataset itself; the *con-urban* area is the overlaid urban area in four datasets, and it is usually the city core area; the *union-urban* area is the model grids which are marked as an urban grid by at least one dataset but not all the four datasets, and it is the union of the urban areas from four datasets except the con-urban area. For the analysis domain (shown in Fig. 1b), the union-urban area fraction is 8.7% in the analysis area, but the con-urban area cover fraction is only 1.6%, which also indicates the great uncertainties of ULUC information in different datasets.

Heat stress indices are widely used for the studies of health risks and biometeorology under heatwave conditions, indicating the “feels-like” temperature, or how hot it really feels (e.g., Buzan et al. 2015; Ma et al. 2018; Sherwood and Matthew 2010). Given the humid summer climate background in the Yangtze River Delta, NOAA’s heat index (HI) was selected for the heat stress analysis of human comfort in this study, and it combines the air temperature and relative humidity to determine the personal perception of the degree of heat, i.e., the body temperature. The HI is also used in the weather forecast on hot, humid summer days by the NOAA national weather service. The HI (unit: °C) is expressed as

$$\text{HI} = c_1 + c_2T + c_3R + c_4TR + c_5T^2 + c_6R^2 + c_7T^2R + c_8TR^2 + c_9T^2R^2$$

where  $R$  is the relative humidity (unit: %) and  $c_1$ – $c_9$  are the empirical parameters. In this paper, the threshold of the danger condition is 41 °C and the threshold value of the extreme caution is 32 °C ([https://en.wikipedia.org/wiki/Heat\\_index](https://en.wikipedia.org/wiki/Heat_index); [https://www.wpc.ncep.noaa.gov/html/heatindex\\_equation.shtml](https://www.wpc.ncep.noaa.gov/html/heatindex_equation.shtml)).

### 3 Results

#### 3.1 Model validations

The observations of the heatwave episode (10 July to 15 August 2013) at 121 meteorological stations in the analysis domain were used to evaluate the model performances in different ULUC experiments as shown in Fig. 2 and Table 3. The model results were interpolated to the meteorological station locations using the bilinear interpolation method, then the bias, correlation coefficient ( $R$ ), and root-mean-square error (RMSE) between model simulations and observations were calculated to evaluate the model performances. All the ULUC experiments overestimated the air temperature at 2 m ( $T_{2\text{ m}}$ ) during the heatwave episode; the biases (the simulations minus the observations) of  $T_{2\text{ m}}$  in the ULUC

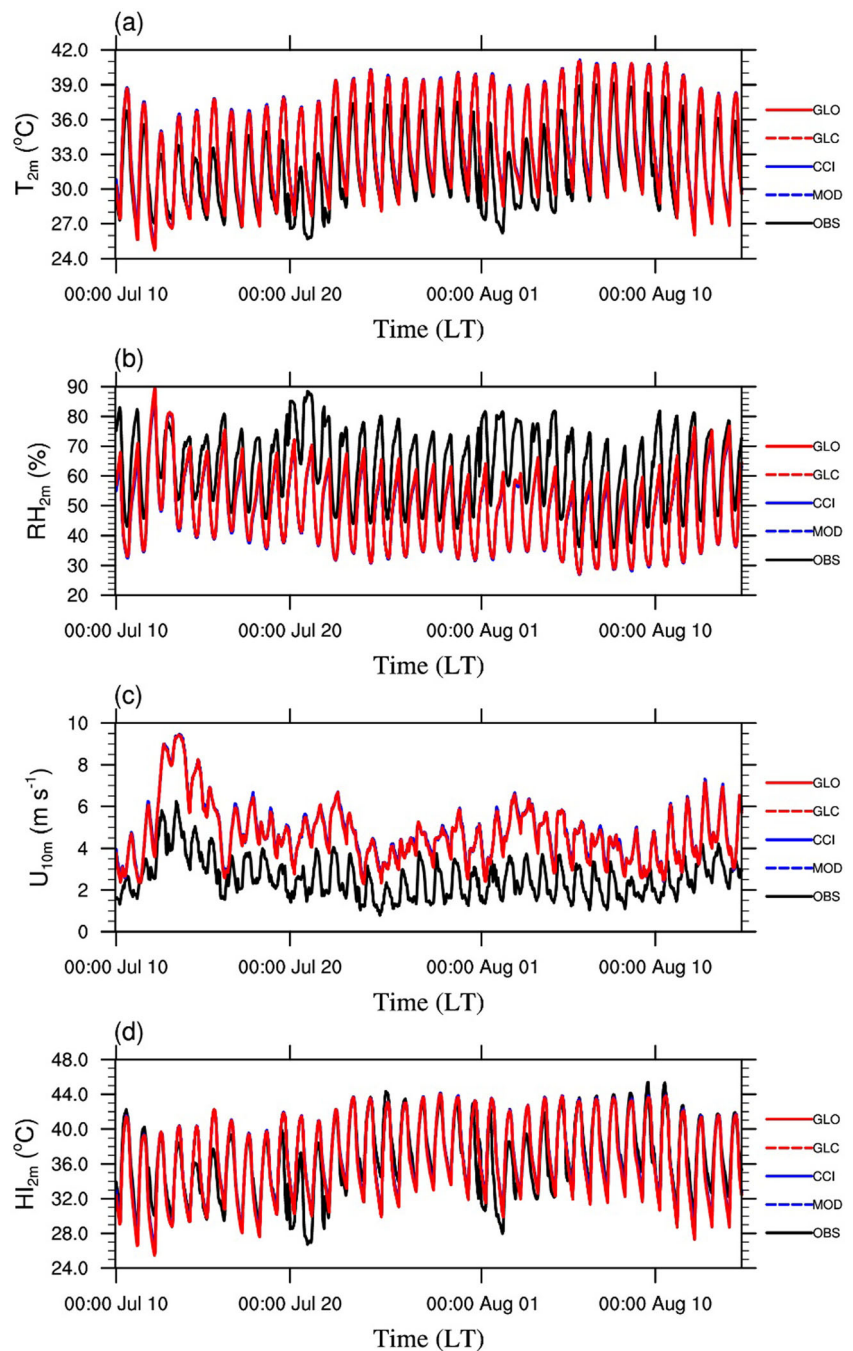
experiments are 1.07 °C in the MOD experiment, 1.09 °C in the CCI experiment, 0.98 °C in the CLC experiment, and 0.97 °C in the GLO experiment, and the RMSEs are 2.02 °C, 2.07 °C, 2.01 °C, and 2.00 °C, respectively. All the ULUC experiments captured the temporal variations, and the  $R$  values are above 0.90. The ULUC experiments overestimated the wind speed at 10 m ( $U_{10\text{ m}}$ ); the biases are 2.29 m s<sup>-1</sup>, 2.27 m s<sup>-1</sup>, 2.20 m s<sup>-1</sup>, and 2.17 m s<sup>-1</sup>, and the RMSEs are 3.02 m s<sup>-1</sup>, 3.01 m s<sup>-1</sup>, 2.95 m s<sup>-1</sup>, and 2.93 m s<sup>-1</sup>, respectively. The relative humidity at 2 m ( $\text{RH}_{2\text{ m}}$ ) of the 121 stations was underestimated in all the ULUC experiments; the biases are 11.16%, 11.51%, 10.66%, 10.51%, 16.07%, 16.38%, 15.77%, and 15.68%, respectively. The underestimation of  $\text{RH}_{2\text{ m}}$  has two reasons: the first one is that the WRF model overestimated  $T_{2\text{ m}}$  as described before, and the second reason is that the specific humidity at 2 m ( $Q_{2\text{ m}}$ ) was underestimated with the biases of -1.45 g kg<sup>-1</sup>, -1.52 g kg<sup>-1</sup>, -1.45 g kg<sup>-1</sup>, and -1.44 g kg<sup>-1</sup> and the RMSEs of 2.25 g kg<sup>-1</sup>, 2.31 g kg<sup>-1</sup>, 2.28 g kg<sup>-1</sup>, and 2.27 g kg<sup>-1</sup>, respectively.

All the observation stations were classified to three types to observe the model performances over different land use types: the union-urban sites (36 sites), the rural sites (51 sites), and the con-urban sites (34 sites) as shown in Table 3. The model performance over the rural area is better than that over the con-urban area and the union-urban area for the simulations of  $T_{2\text{ m}}$ , and the model performance over the union urban area is better than that over other areas for the simulations of  $Q_{2\text{ m}}$  in all the four ULUC experiments. The ULUC experiments have some simulation skills for the  $U_{10\text{ m}}$  and  $\text{RH}_{2\text{ m}}$ . The GLO experiments output the best simulation results usually with the lowest bias and RMSE among the four ULUC experiments, especially for the  $T_{2\text{ m}}$  simulations. For example, the bias of  $T_{2\text{ m}}$  is 0.97 °C at all observation sites and 0.99 °C at the union-urban sites and the RMSEs are 2.00 °C and 1.97 °C respectively.

The simulation HIs were also compared with the values calculated using the respective observations. The ULUC experiments overestimated the HIs at the observation sites with bias ranging from 0.31 to 0.63 °C, but the model performances are different over different land cover type sites. All the ULUC experiments underestimated HI over the rural sites due to the less overestimated  $T_{2\text{ m}}$  and less underestimated  $\text{RH}_{2\text{ m}}$ , and the models overestimated HI over the union-urban and con-urban sites because of the overestimation of  $T_{2\text{ m}}$  over these sites.

The spatial distribution of the July–August average  $T_{2\text{ m}}$  (Fig. 3) also showed that the observed highest mean  $T_{2\text{ m}}$  occurred in south Zhejiang Province which was higher than 32 °C and the WRF model captured the high-temperature core well in all the experiments while with a 2 °C overestimation. The most obvious bias took place in the northern part of the analysis area where all the experiments overestimated the air temperature due to the overestimated surface skin temperature

**Fig. 2** The comparisons between the observations and the simulations of **a** air temperature at 2 m, **b** relative humidity at 2 m, **c** wind speed at 10 m, and **d** heat index at 2 m



(TSK) simulations as shown below. The most obvious difference among the four ULUC experiments is that the CCI experiment outputted higher  $T_{2m}$  over the urban area especially over Shanghai City than the others did. The results in both  $T_{2m}$  and TSK indicate that using different ULUC datasets will lead to differences in the simulations, but it is hard to distinguish which dataset performances are better due to the lack of density observations in urban areas.

The simulated TSK was also compared to the MODIS satellite TSK products, and the simulated surface skin temperature at respective hours was selected to compare to the

daytime and nocturnal surface skin temperature as shown in Figs. 4 and 5. Strong urban heat island occurred over urban areas both in daytime and at night. All the ULUC experiments captured the spatial characteristics of the UHI distributions, the correlation coefficients were greater than 0.98, but all the ULUC experiments overestimated TSK, the bias between the ULUC experiments, and the MODIS observations in the daytime are about 3.0  $^{\circ}\text{C}$  for the daytime simulation and 2.8  $^{\circ}\text{C}$  for the nighttime simulation especially in the northern part of the analysis domain (for daytime TSK) and over cities (for nocturnal TSK).

**Table 3** Evaluations of model performances

	$T_2$ m				$U_{10}$ m				$RH_2$ m				$Q_2$ m				HI			
	Bias (°C)		RMSE (°C)		Bias (m s <sup>-1</sup> )		RMSE (m s <sup>-1</sup> )		Bias (%)		RMSE (%)		Bias (g kg <sup>-1</sup> )		RMSE (g kg <sup>-1</sup> )		Bias (°C)		RMSE (°C)	
	R	R	R	R	R	R	R	R	R	R	R	R	R	R	R	R	R	R	R	
<b>All sites</b>																				
MOD	1.07	2.02	0.91	2.29	3.02	0.45	-11.16	16.07	0.72	-1.45	2.25	0.78	0.63	2.31	0.75					
CCI	1.09	2.07	0.90	2.27	3.01	0.45	-11.51	16.38	0.72	-1.52	2.31	0.78	0.65	2.36	0.74					
GLC	0.98	2.02	0.91	2.20	2.95	0.47	-11.66	15.77	0.72	-1.45	2.28	0.77	0.44	2.34	0.74					
GLO	0.97	2.00	0.90	2.17	2.93	0.47	-11.51	15.68	0.72	-1.44	2.27	0.77	0.41	2.35	0.74					
<b>Con-urban sites</b>																				
MOD	1.49	2.02	0.91	2.51	3.15	0.42	-12.53	15.23	0.73	-1.07	1.85	0.75	1.89	2.09	0.75					
CCI	1.51	2.09	0.91	2.47	3.13	0.43	-12.53	15.54	0.73	-1.07	1.88	0.75	2.04	2.09	0.75					
GLC	1.39	1.87	0.92	2.36	3.05	0.45	-11.32	15.58	0.74	-0.97	1.81	0.74	1.74	2.07	0.76					
GLO	1.37	1.82	0.92	2.33	3.03	0.45	-11.16	15.49	0.74	-0.96	1.81	0.74	1.68	2.05	0.76					
<b>Rural sites</b>																				
MOD	0.65	1.95	0.90	2.15	2.95	0.47	-9.90	15.71	0.71	-1.74	2.71	0.73	-0.48	2.60	0.73					
CCI	0.79	1.82	0.90	2.16	2.95	0.47	-10.22	16.00	0.71	-1.74	2.71	0.73	-0.40	2.62	0.73					
GLC	0.64	1.70	0.90	2.14	2.94	0.48	-9.72	15.64	0.71	-1.74	2.71	0.73	-0.51	2.62	0.73					
GLO	0.65	1.70	0.90	2.12	2.93	0.48	-9.63	15.61	0.71	-1.73	2.71	0.73	-0.54	2.63	0.73					
<b>Union-urban sites</b>																				
MOD	1.14	1.95	0.91	2.27	3.01	0.46	-11.53	16.27	0.73	-1.44	2.11	0.78	0.75	2.21	0.75					
CCI	1.13	2.11	0.90	2.27	3.01	0.46	-11.92	16.58	0.72	-1.59	2.25	0.77	0.66	2.33	0.74					
GLC	1.01	1.99	0.90	2.15	2.91	0.47	-11.01	16.00	0.73	-1.51	2.21	0.77	0.44	2.29	0.74					
GLO	0.99	1.97	0.90	2.11	2.88	0.47	-10.81	15.87	0.72	-1.50	2.19	0.77	0.39	2.30	0.74					

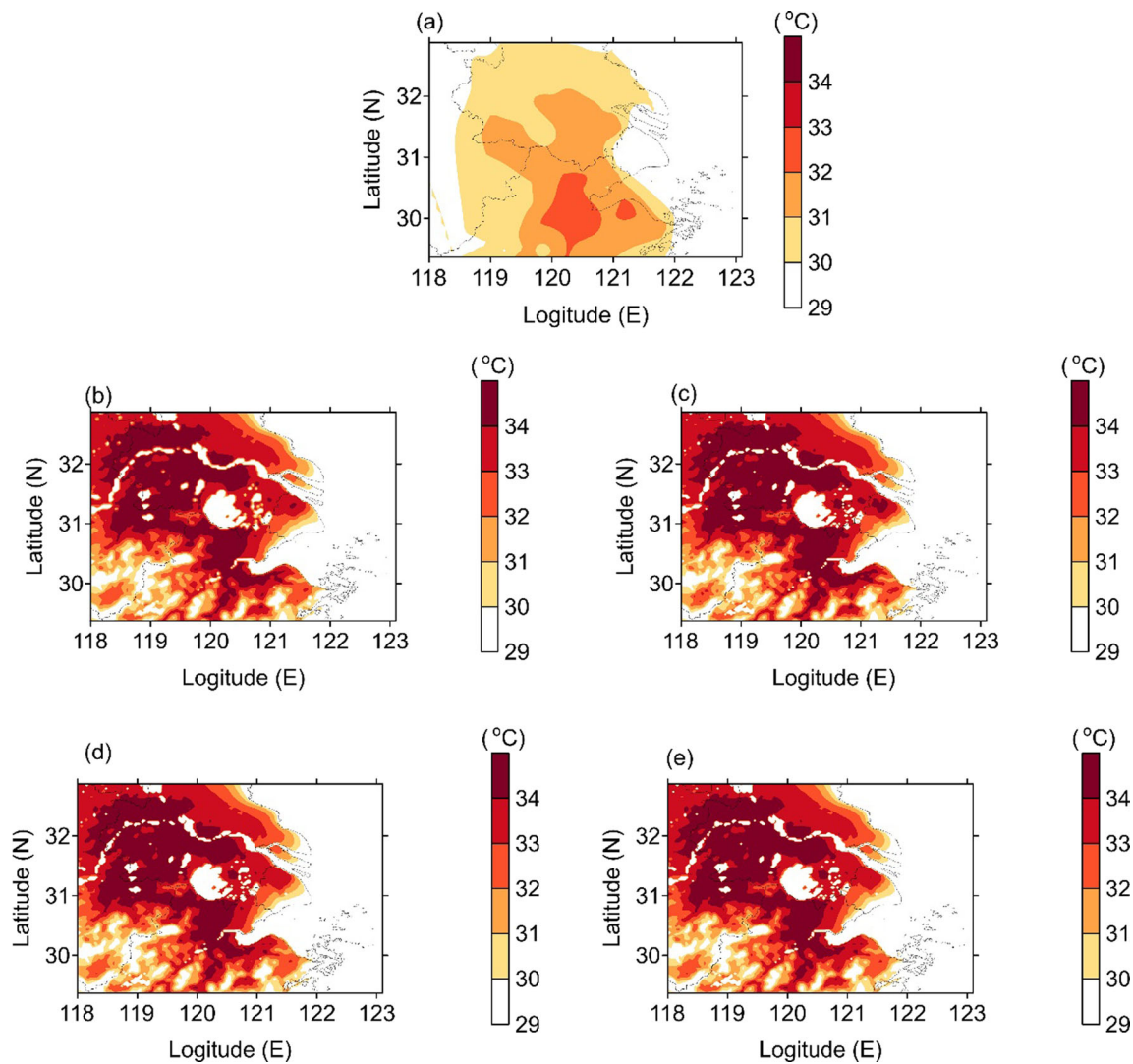


**Fig. 3** Average air temperature at 2 m. **a** Station observations and simulation results of **b** MOD, **c** CCI, **d** GLC, and **e** GLO

### 3.2 ULUC uncertainty impacts on the simulations of urban warming effects and heat index

The urbanization-induced land cover changes the surface radiation and thermal features, and this results in an increase in both surface skin temperature and near-surface temperature and usually named “urban warming effect.” The differences of TSK and  $T_{2\text{ m}}$  between the ULUC experiments and the NOURBN experiment were used to observe the urban warming effect simulated using different ULUC datasets (Fig. 6). The simulated average land surface skin temperatures of July–August over the analysis area were about 34.7–34.8 °C, the average TSK values over urban grids were 2.7–3.0 °C higher than those over the vegetation land surface, and the MOD experiment outputted the greatest average daily maximum over urban grids with the values of 43.04 °C. The differences between the ULUC experiments and the NOURBN experiment showed that the urban warming effect in TSK

was very significant, and the TSK increasing over the whole analysis area was only 0.18 (in the GLO experiment) to 0.31 °C (in the CCI experiment), because the urban land coverage fraction is relatively low (less than 10% even in the CCI experiment). But, the average increases over the own-urban area are 2.38 °C, 2.44 °C, 2.41 °C, and 2.27 °C; the increases over the con-urban area are 2.85 °C, 3.21 °C, 2.84 °C, and 2.68 °C; and the increases over the union-urban area are 1.28 °C, 1.94 °C, 1.23 °C, and 1.12 °C. The urban warming effect also occurred in the near-surface air temperature but weaker than that in the surface skin temperature. The average  $T_{2\text{ m}}$  differences between the ULUC experiments and the NOURBN experiment are only from 0.11 to 0.18 °C, while the average differences were 0.66 °C, 0.79 °C, 0.73 °C, and 0.65 °C over the own-urban area; 0.92 °C, 1.16 °C, 0.95 °C, and 0.85 °C over the con-urban area; and 0.42 °C, 0.67 °C, 0.46 °C, and 0.39 °C over the union-urban area in the respective ULUC experiments (i.e., MOD, CCI, GLC, and GLO). The urban



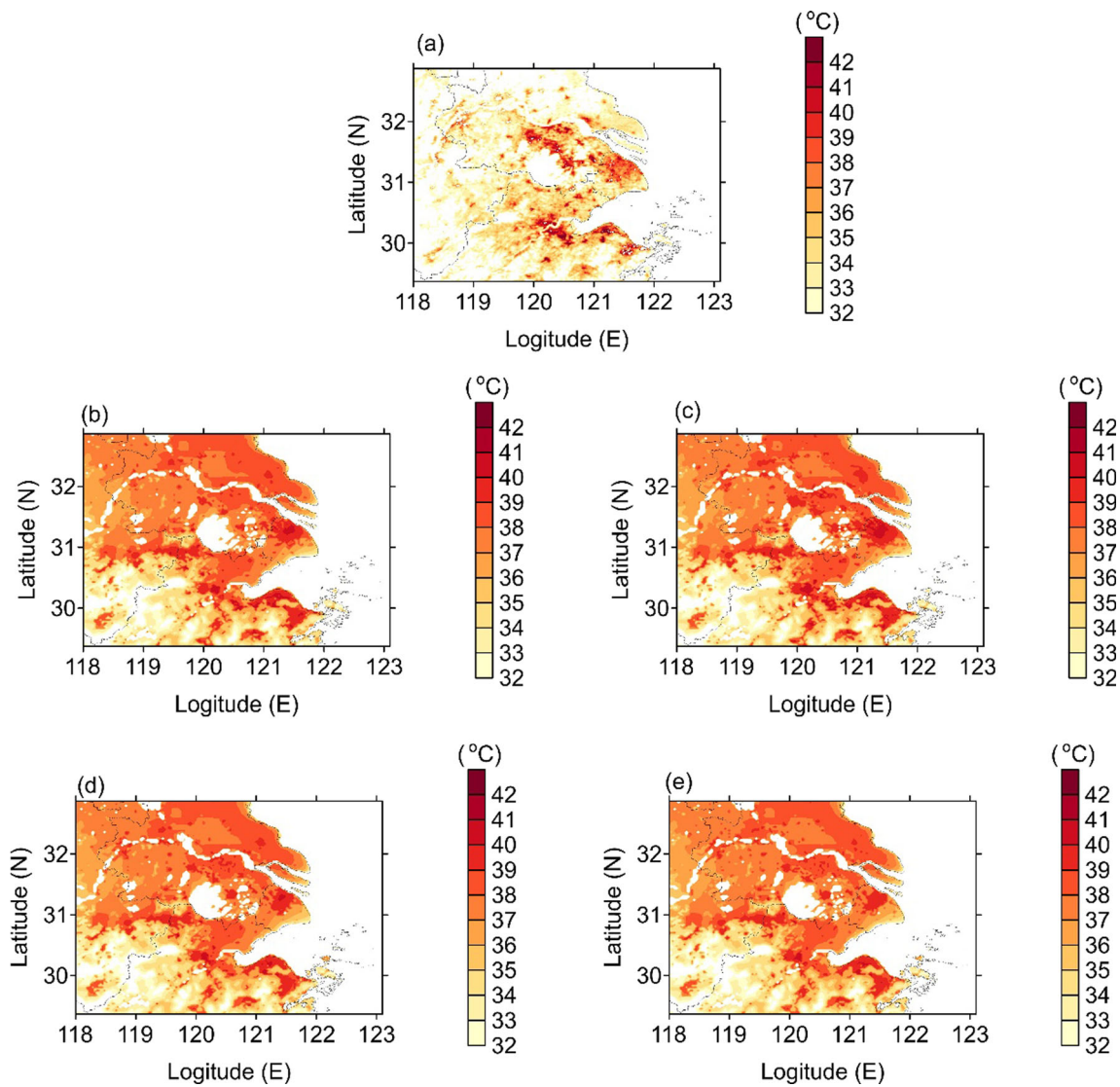


Fig. 4 The same as Fig. 3 but for the daytime surface skin temperature

warming effect is greater over the con-urban area than over the own-urban area, because the con-urban area includes a higher fraction of high-density urban grids. Both the changes in TSK and  $T_{2\text{ m}}$  indicated regional effects, and the EIs were 1.94, 2.40, 2.41, and 1.87 in TSK and 2.34, 2.88, 3.11, and 2.31 in the air temperature at 2 m; the EIs in  $T_{2\text{ m}}$  were greater than those in TSK due to the advection of near-surface atmosphere.

As documented in previous researches (Zhang et al. 2010), the urban warming effect is more significant on the daily minimum TSK and  $T_{2\text{ m}}$  than on the daily maximum TSK and  $T_{2\text{ m}}$ , and this results in a decrease in the diurnal ranges in TSK and  $T_{2\text{ m}}$  (Fig. 7). The decreases in the diurnal range of TSK were  $-0.94$ ,  $-1.19$ ,  $-1.09$ , and  $-1.00$  over the own-urban area;  $-2.89$ ,  $-4.10$ ,  $-2.75$ , and  $-2.43$  over the con-urban area; and  $-0.57$ ,  $-0.98$ ,  $-0.62$ , and  $-0.55$  over the union-urban area; the decreases in the diurnal range of  $T_{2\text{ m}}$  were  $-$

$0.83$ ,  $-0.97$ ,  $-0.97$ , and  $-0.79$  over the own-urban area;  $-1.59$ ,  $-2.07$ ,  $-1.65$ , and  $-1.50$  over the con-urban area; and  $-0.49$ ,  $-0.79$ ,  $-0.54$ , and  $-0.44$  over the union-urban area. Urbanization impacts on the diurnal ranges of TSK and  $T_{2\text{ m}}$  both showed regional influences; the EIs of the diurnal range of TSK were 2.10, 2.05, 2.25, and 1.92; and the EIs of the diurnal range of  $T_{2\text{ m}}$  were 2.28, 2.64, 2.83, and 2.30.

Figure 8 a–d illustrate the simulated spatial distribution of the mean HI during the 10 July to 15 August heatwave episode as shown in Fig. 2. It is clear that the mean HI over the whole analysis domain reached the caution level in all the ULUC experiments with the values greater than  $27\text{ }^{\circ}\text{C}$  except some coastal and mountainous area. The mean HI over most part of the domain reached the extreme caution level with the value greater than  $32\text{ }^{\circ}\text{C}$ . The spatial average HI over the analysis domain is  $36.4\text{ }^{\circ}\text{C}$  in the heatwave episode, and the

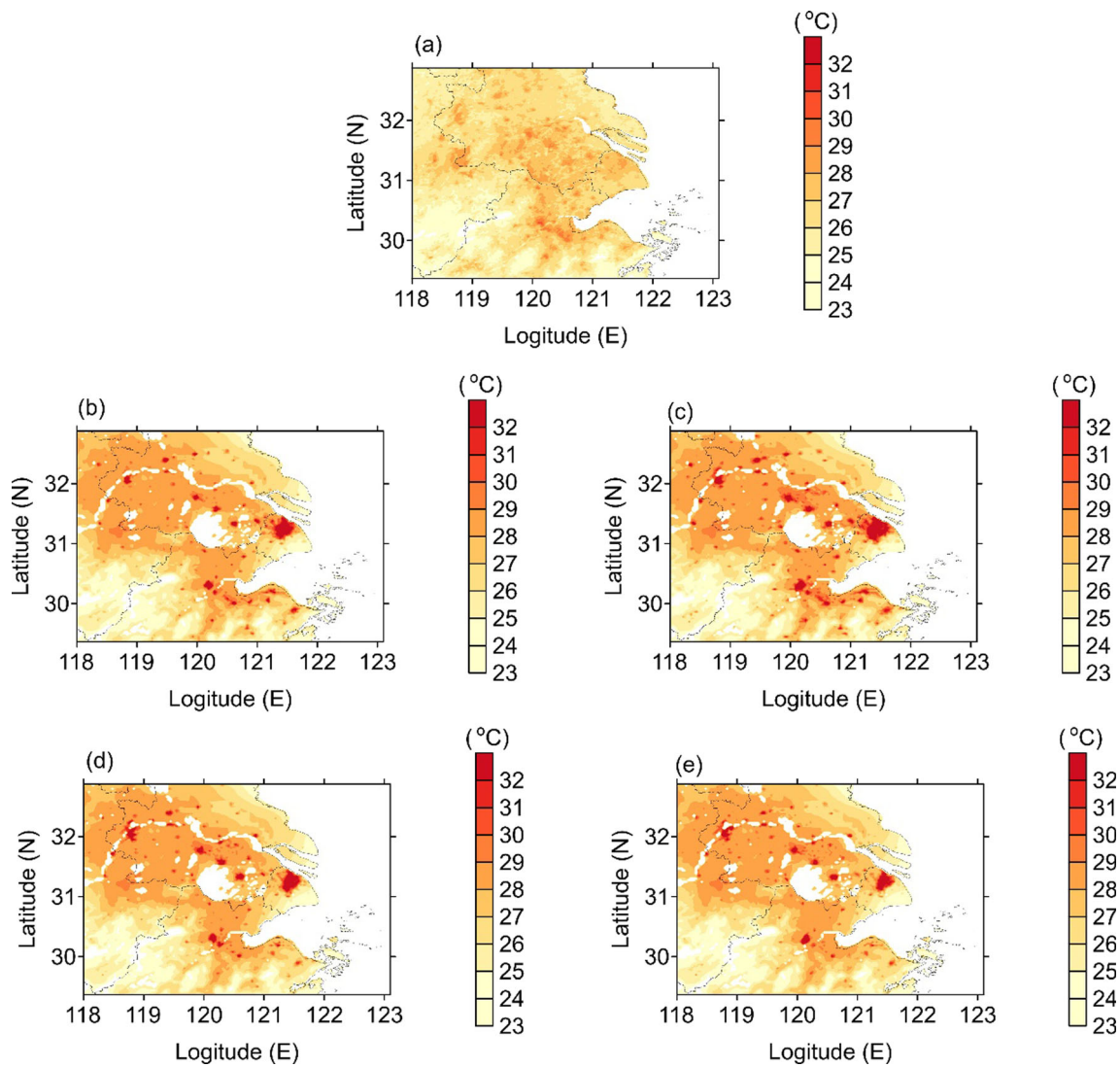


**Fig. 5** The same as Fig. 2 but for the nocturnal surface skin temperature

mean value over the own-urban area is 39.6 °C. The HI is controlled by  $T_{2\text{ m}}$  and  $\text{RH}_{2\text{ m}}$ , and it has a similar diurnal variation of  $T_{2\text{ m}}$  and usually reaches its maximum at 14:00 LT. The spatial average HI at 14:00 LT over the analysis domain is 41.0 °C, indicating that it should be extremely cautionary for outdoor activities at this time (figures not shown here). The maximum of the average HI at 14:00 LT over the own-urban area was 2 °C higher than the spatial average. The differences in the HI between the ULUC experiments and the NOURB experiment illustrated the influence of urbanization; the differences in the average HI of the heatwave episodes over the own-urban area are 0.68 °C in the MOD experiment, 0.83 °C in the CCI experiment, 0.79 °C in the GLC experiment, and 0.68 °C in the GLO experiment, and the maximum of the average HI differences is 2.2, 3.4, 2.1, and 2.0 °C, respectively (Fig. 8e–h).

The occurrence frequencies of extreme caution and danger conditions in the heatwave episode were calculated with the hourly outputs of HI. The occurrence frequency of the

extreme caution condition increased 15% over the city core areas, and the frequency of danger condition increased about 5% as well as in all the ULUC experiments due to the urbanization effects (Fig. 9). The greatest increase appeared in the CCI experiments due to the highest urban land cover fraction among the four experiments. The regional influence of urban warming effect in  $T_{2\text{ m}}$  also caused urbanization regional influence effects in the HI and its occurrence frequencies, so the spatial distribution patterns of their differences between the ULUC experiment and the NOURB experiment are similar to those of the differences in  $T_{2\text{ m}}$ .

### 3.3 Impacts on surface energy balance simulations

The energy heat exchange between the land surface and the atmosphere over the urban area is always dominated by sensible heat flux due to the low surface soil moisture and little vegetation coverage (Fig. 10). In the ULUC experiments, the

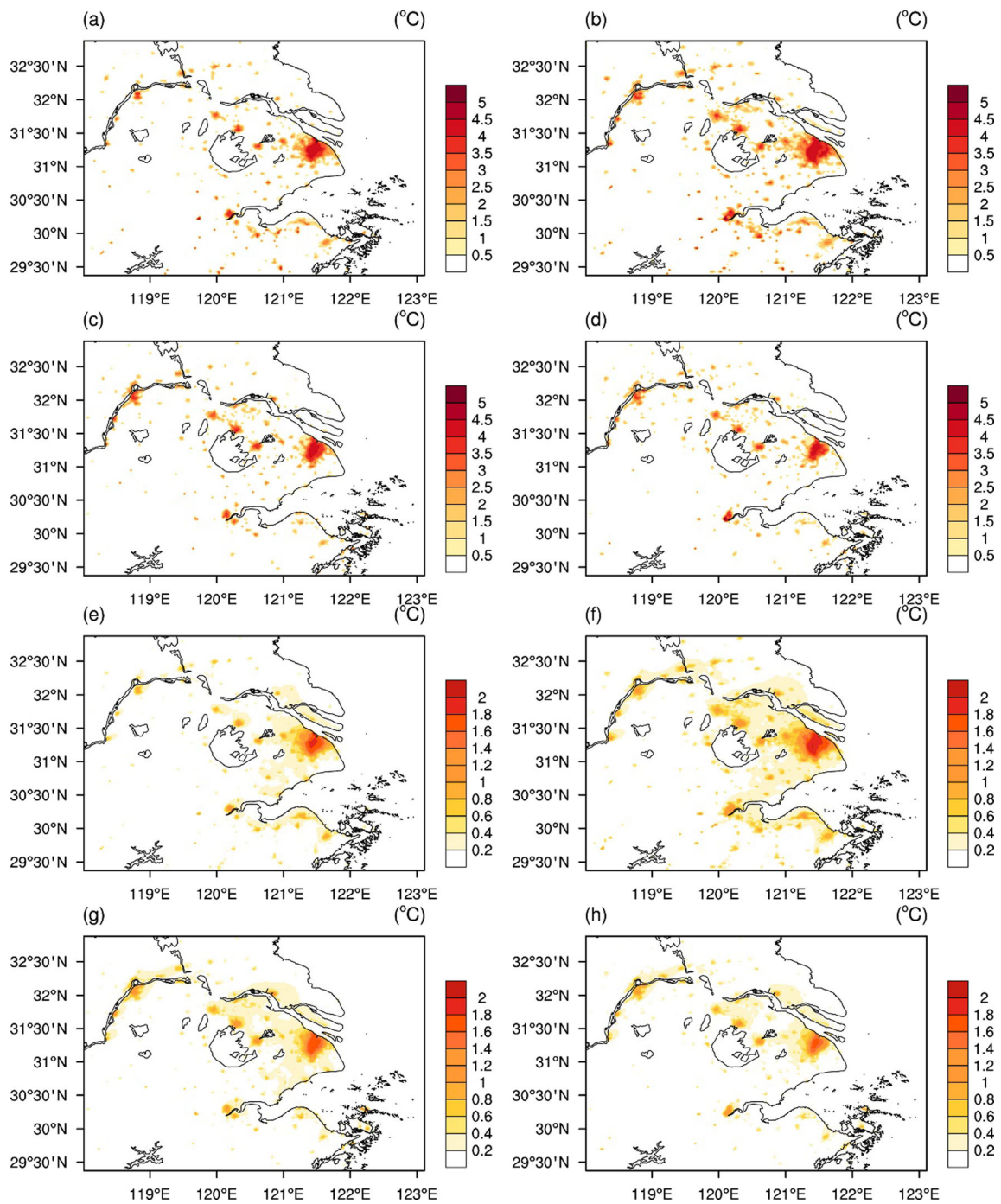


**Fig. 6** The differences in the simulated average TSK between the a MOD, b CCI, c GLC, and d GLO experiments and the NOURB experiment and the differences in the simulated average T<sub>2m</sub> between the e MOD, f CCI, g GLC, and h GLO experiments and the NOURB experiment

CCI experiment outputted the greatest spatial average land surface sensible heat flux over the analysis domain in the heatwave episode with a value of 118.61 W m<sup>-2</sup> because the ESA CCI dataset showed the largest urban land cover area as shown in Table 4; the MOD experiment outputted the second greatest average value of 117.18 W m<sup>-2</sup>, and the results from the GLC and GLO experiment were close with values of 116.96 W m<sup>-2</sup> and 116.83 W m<sup>-2</sup>, respectively. The coastal

area in the northern part of analysis showed relatively higher sensible heat fluxes than the other rural areas, because of the higher simulated TSK and the lower T<sub>2m</sub> due to advection from the sea, and it leads to a higher-temperature gradient between land surface and near-surface atmosphere. The urban area average sensible heat flux was much higher than the analysis domain average; the maximum average value all occurred on the urban grids, and the values were 212.63 W m<sup>-2</sup>

**Table 4** Simulated average, maximum, minimum, and differences between the NOURB experiment and EIs of the land surface and near-surface variables

	Avg	Max	Min	Avg <sub>own-urban</sub>	Max <sub>own-urban</sub>	Min <sub>own-urban</sub>	Diff	Diff <sub>own-urban</sub>	EI
Surface sensible heat flux ( $\text{W m}^{-2}$ )									
MOD	117.3	213.0	67.9	175.3	213.0	153.0	2.1	47.9	1.00
CCI	118.6	210.9	67.9	172.5	210.9	143.0	2.9	45.7	1.00
GLC	117.0	210.8	67.9	174.1	208.4	142.6	1.6	45.3	1.01
GLO	116.8	208.4	67.9	172.8	210.8	148.0	1.5	45.7	1.01
Surface latent heat flux ( $\text{W m}^{-2}$ )									
MOD	54.9	122.7	0.8	1.9	14.5	0.8	-1.8	-39.2	1.00
CCI	53.7	122.7	0.9	2.6	20.8	0.9	-2.5	-38.1	0.99
GLC	55.1	122.7	0.7	2.5	25.4	0.7	-1.3	-35.9	1.00
GLO	55.2	122.7	0.7	2.5	18.8	0.7	-1.3	-36.8	1.00
Surface skin temperature ( $^{\circ}\text{C}$ )									
MOD	34.8	41.8	25.2	37.8	41.8	30.8	0.17	2.55	2.50
CCI	34.8	41.7	25.2	37.6	41.7	30.5	0.21	2.36	2.40
GLC	34.7	41.2	25.2	37.5	41.1	30.2	0.13	2.21	2.47
GLO	34.7	41.4	25.2	37.4	41.4	30.0	0.11	2.16	1.84
Air temperature at 2 m ( $^{\circ}\text{C}$ )									
MOD	32.7	35.6	24.0	33.7	35.6	25.9	0.10	0.70	3.15
CCI	32.8	35.7	24.0	33.8	35.7	26.6	0.12	0.76	2.88
GLC	32.7	35.5	24.0	33.7	35.5	26.0	0.08	0.65	3.11
GLO	32.7	35.6	24.0	33.7	35.6	25.4	0.06	0.59	2.31
Specific humidity at 2 m ( $\text{g kg}^{-1}$ )									
MOD	15.9	19.4	15.2	15.8	18.9	15.2	-0.03	-0.22	1.31
CCI	15.9	19.4	15.2	15.7	18.8	15.2	-0.04	-0.23	1.69
GLC	15.9	19.4	15.2	15.8	18.7	15.2	-0.02	-0.20	1.30
GLO	15.9	19.4	15.2	15.7	18.7	15.2	-0.02	-0.19	1.20
Relative humidity at 2 m (%)									
MOD	53.0	96.8	43.5	50.7	86.5	43.5	-0.42	-3.06	2.38
CCI	52.9	96.8	43.6	50.1	86.6	43.1	-0.52	-3.03	2.26
GLC	53.1	96.9	43.5	50.7	86.8	43.6	-0.32	-2.70	2.25
GLO	53.2	96.8	43.5	50.5	89.8	43.5	-0.27	-2.48	1.71

in the MOD experiment,  $210.87 \text{ W m}^{-2}$  in the CCI experiment,  $208.43 \text{ W m}^{-2}$  in the GLC experiment, and  $210.81 \text{ W m}^{-2}$  in the GLO experiment. The averages over the own-urban area were close with the values of  $173.64 \text{ W m}^{-2}$ ,  $172.46 \text{ W m}^{-2}$ ,  $174.10 \text{ W m}^{-2}$ , and  $172.82 \text{ W m}^{-2}$ ; the averages over the con-urban area were about  $10 \text{ W m}^{-2}$  greater than those over the own-urban area; and the values were  $183.73 \text{ W m}^{-2}$ ,  $187.73 \text{ W m}^{-2}$ ,  $182.02 \text{ W m}^{-2}$ , and  $180.50 \text{ W m}^{-2}$ , respectively, over the union-urban area; the values were  $149.01 \text{ W m}^{-2}$ ,  $161.63 \text{ W m}^{-2}$ ,  $147.52 \text{ W m}^{-2}$ , and  $146.28 \text{ W m}^{-2}$ , respectively. In this heatwave episode, the land surface latent heat flux was relatively low due to the low soil moisture. In all the sensitivity experiments, the analysis domain average land surface average latent heat flux was only approximately half of the sensible heat flux, and the value was  $54.88 \text{ W m}^{-2}$ ,

$53.73 \text{ W m}^{-2}$ ,  $55.14 \text{ W m}^{-2}$ , and  $55.25 \text{ W m}^{-2}$ ; the maximum July–August average happened over the vegetated grid, with values around  $123 \text{ W m}^{-2}$ , while the minimum occurred over the city core grid with values less than  $1 \text{ W m}^{-2}$ . The urban area averages were also very small; the averages over the own-urban area were  $1.94 \text{ W m}^{-2}$ ,  $2.59 \text{ W m}^{-2}$ ,  $2.51 \text{ W m}^{-2}$ , and  $2.48 \text{ W m}^{-2}$ ; and the averages over the con-urban area were  $1.08 \text{ W m}^{-2}$ ,  $0.87 \text{ W m}^{-2}$ ,  $1.44 \text{ W m}^{-2}$ , and  $1.59 \text{ W m}^{-2}$ , respectively. The averages over the union-urban area were relatively larger with the values of  $21.68 \text{ W m}^{-2}$ ,  $11.78 \text{ W m}^{-2}$ ,  $23.60 \text{ W m}^{-2}$ , and  $24.42 \text{ W m}^{-2}$  because the area includes some vegetation-covered grids due to the different urban sprawling in different datasets.

All the ULUC experiments showed that the urbanization-induced land cover changes led to higher

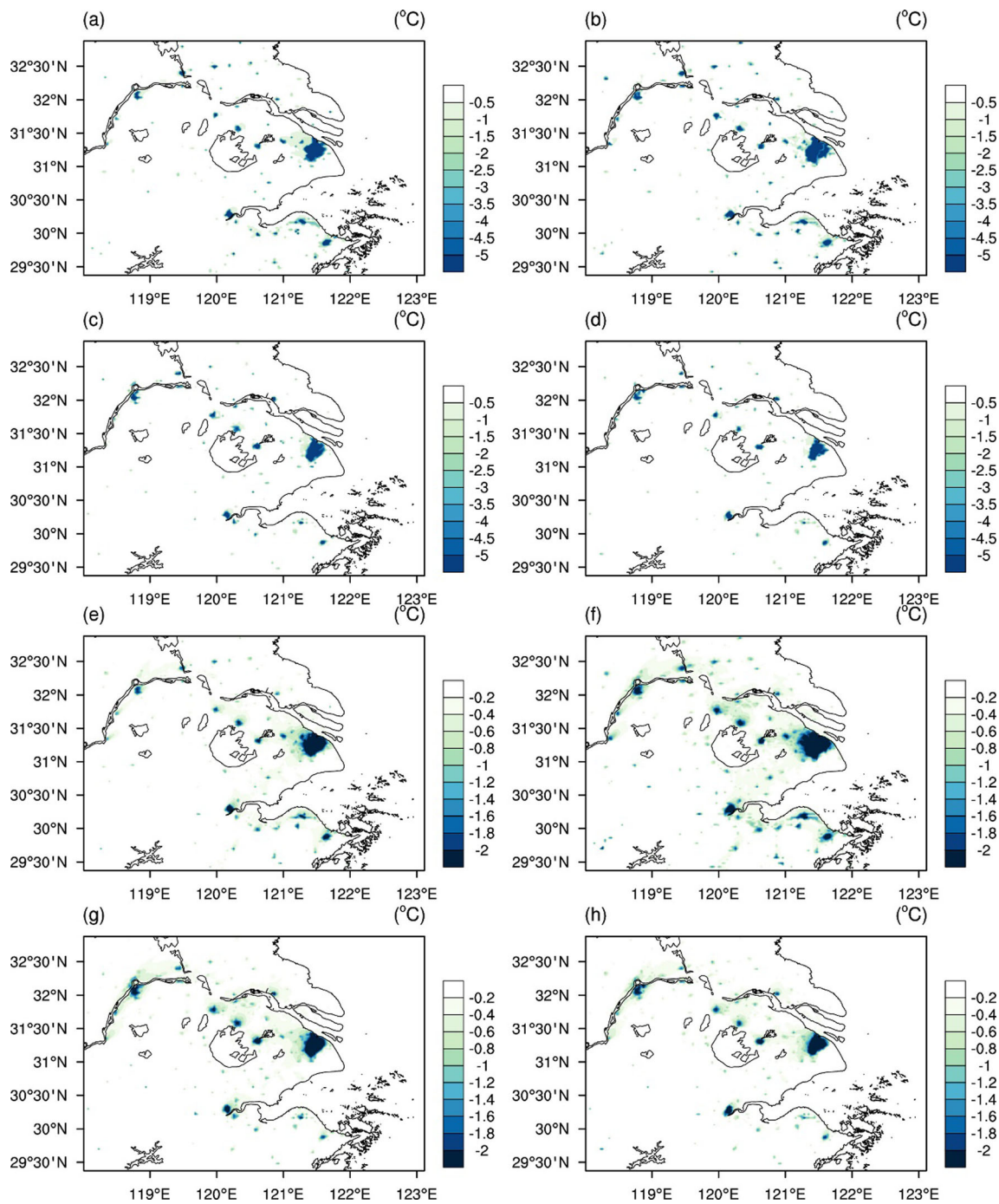


**Fig. 7** The differences in the simulated average diurnal variation range of TSK between the **a** MOD, **b** CCI, **c** GLC, and **d** GLO experiments and the NOURB experiment and the differences in the simulated average

diurnal variation range of  $T_{2m}$  between the **e** MOD, **f** CCI, **g** GLC, and **h** GLO experiments and the NOURB experiment

sensible heat flux and lower latent heat flux over the urbanized area compared to the NOURB experiment due to the higher heat cavity and lower soil moisture caused by the impervious urban land cover. The urbanization caused an increase in the surface sensible heat flux over the whole analysis area, and the difference averages were  $2.90 \text{ W m}^{-2}$ ,  $4.33 \text{ W m}^{-2}$ ,  $2.68 \text{ W m}^{-2}$ , and  $2.55 \text{ W m}^{-2}$  in the MOD, CCI, GLC, and CLO experiments, respectively;

the biggest change also occurred in the CCI experiments (Fig. 11). The spatial average differences between the ULUC experiments and the NOURB experiment were  $47.9 \text{ W m}^{-2}$ ,  $45.7 \text{ W m}^{-2}$ ,  $45.3 \text{ W m}^{-2}$ , and  $45.7 \text{ W m}^{-2}$  over the own-urban area;  $60.10 \text{ W m}^{-2}$ ,  $64.09 \text{ W m}^{-2}$ ,  $58.38 \text{ W m}^{-2}$ , and  $56.87 \text{ W m}^{-2}$  over the con-urban area; and  $24.98 \text{ W m}^{-2}$ ,  $37.61 \text{ W m}^{-2}$ ,  $23.50 \text{ W m}^{-2}$ , and  $22.25 \text{ W m}^{-2}$  over the union-urban area. The

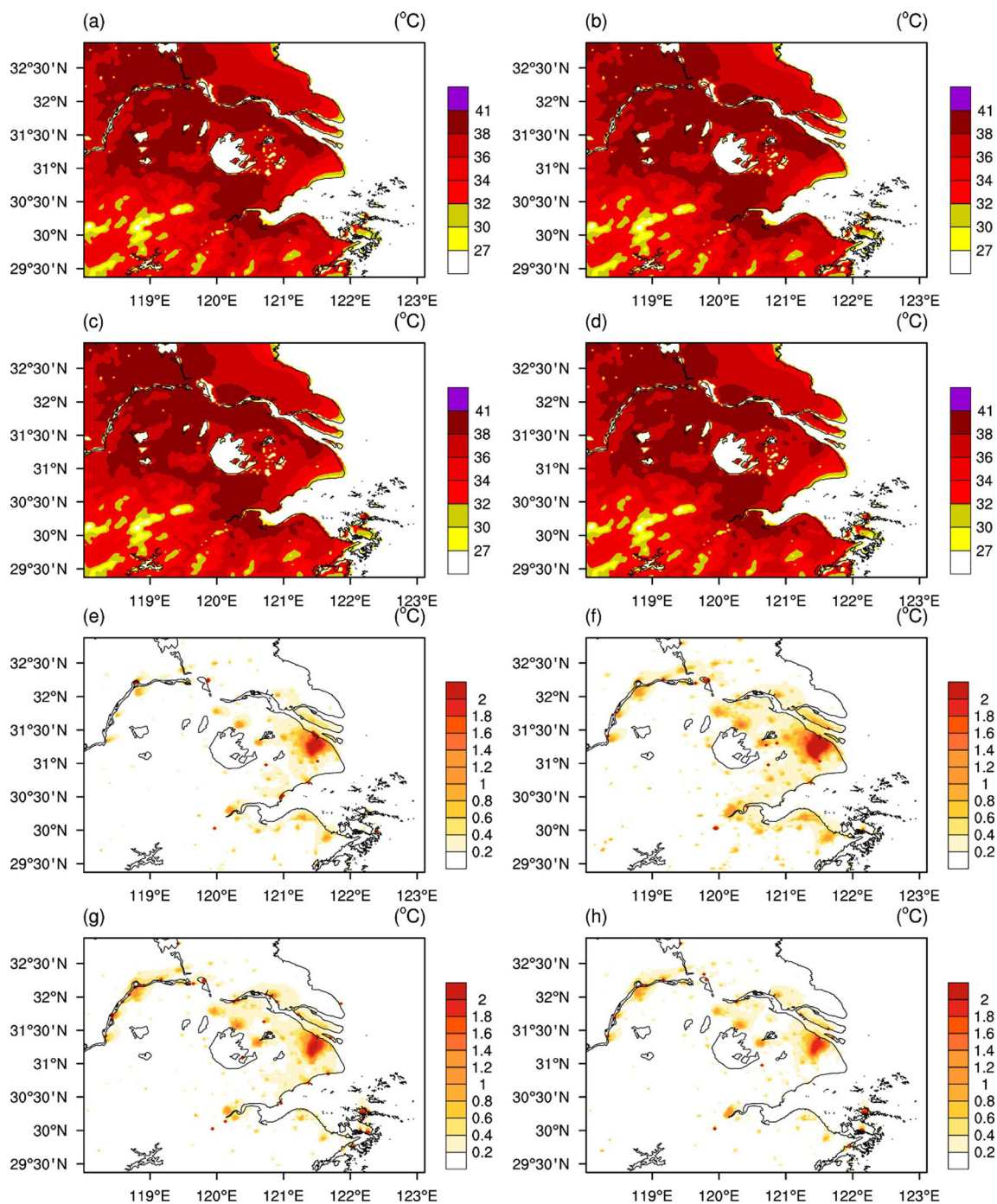


**Fig. 8** The simulated mean HI during the heatwave episode of 10 July to 15 August 2013 in the **a** MOD, **b** CCI, **c** GLC, and **d** GLO experiments and the differences in the HI between the **e** MOD, **f** CCI, **g** GLC, and **h** GLO experiments and the NOURB experiment

urbanization-induced land cover changes also resulted in a decrease in the surface latent heat flux, and the mean differences over the land surface in the analysis area were  $-2.49 \text{ W m}^{-2}$ ,  $-3.64 \text{ W m}^{-2}$ ,  $-2.22 \text{ W m}^{-2}$ , and  $-2.12 \text{ W m}^{-2}$  in the MOD, CCI, GLC, and GLO experiments, respectively; much more dramatic changes occurred over the urban area, and the spatial average differences between the ULCU experiments and the NOURB experiment were  $-$

$40.14 \text{ W m}^{-2}$ ,  $-38.89 \text{ W m}^{-2}$ ,  $-39.13 \text{ W m}^{-2}$ , and  $-38.60 \text{ W m}^{-2}$  over the own-urban area;  $-40.42 \text{ W m}^{-2}$ ,  $-40.64 \text{ W m}^{-2}$ ,  $-40.06 \text{ W m}^{-2}$ , and  $-39.91 \text{ W m}^{-2}$  over the con-urban area; and  $-20.44 \text{ W m}^{-2}$ ,  $-30.33 \text{ W m}^{-2}$ ,  $-18.51 \text{ W m}^{-2}$ , and  $-17.70 \text{ W m}^{-2}$  over the union-urban area. The EIs of both surface sensible heat flux and latent heat flux were close to 1.0 which indicated that the changes only occurred over the urban area.

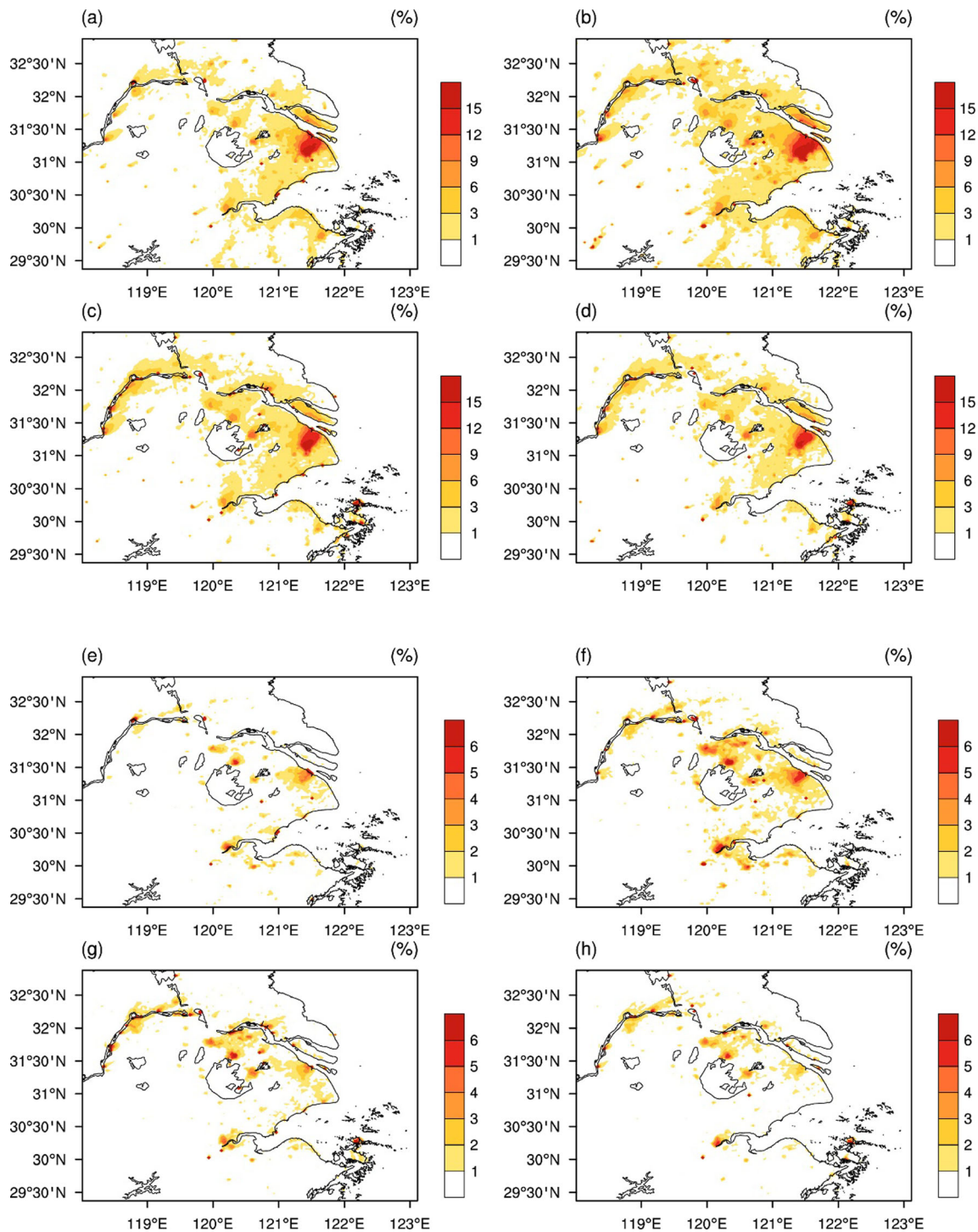


**Fig. 9** The differences in the occurrence frequency of the extreme caution condition ( $HI > 32^\circ$ ) in the heatwave episode in the **a** MOD, **b** CCI, **c** GLC, and **d** GLO experiments and the NOURB experiment and the

occurrence frequency of the danger condition ( $HI > 41^\circ$ ) between the **e** MOD, **f** CCI, **g** GLC, and **h** GLO experiments and the NOURB experiment

### 3.4 Impacts on near-surface humidity

The urbanization-induced land cover changes reduced the evapotranspiration of land surface; this led to a decrease in the surface latent heat flux and caused lower near-surface humidity over the urban area (Fig. 12). This phenomenon is

usually named as “urban dry island.” In all the ULUC experiments, the spatial average near-surface-specific humidity was about  $15.9 \text{ g kg}^{-1}$  and the urban area average was about  $15.7 \text{ g kg}^{-1}$ . The mean differences over the land surface in the whole analysis domain between the ULUC experiments and the NOURB experiment were very tiny, only  $-0.03 \text{ g kg}^{-1}$ , -

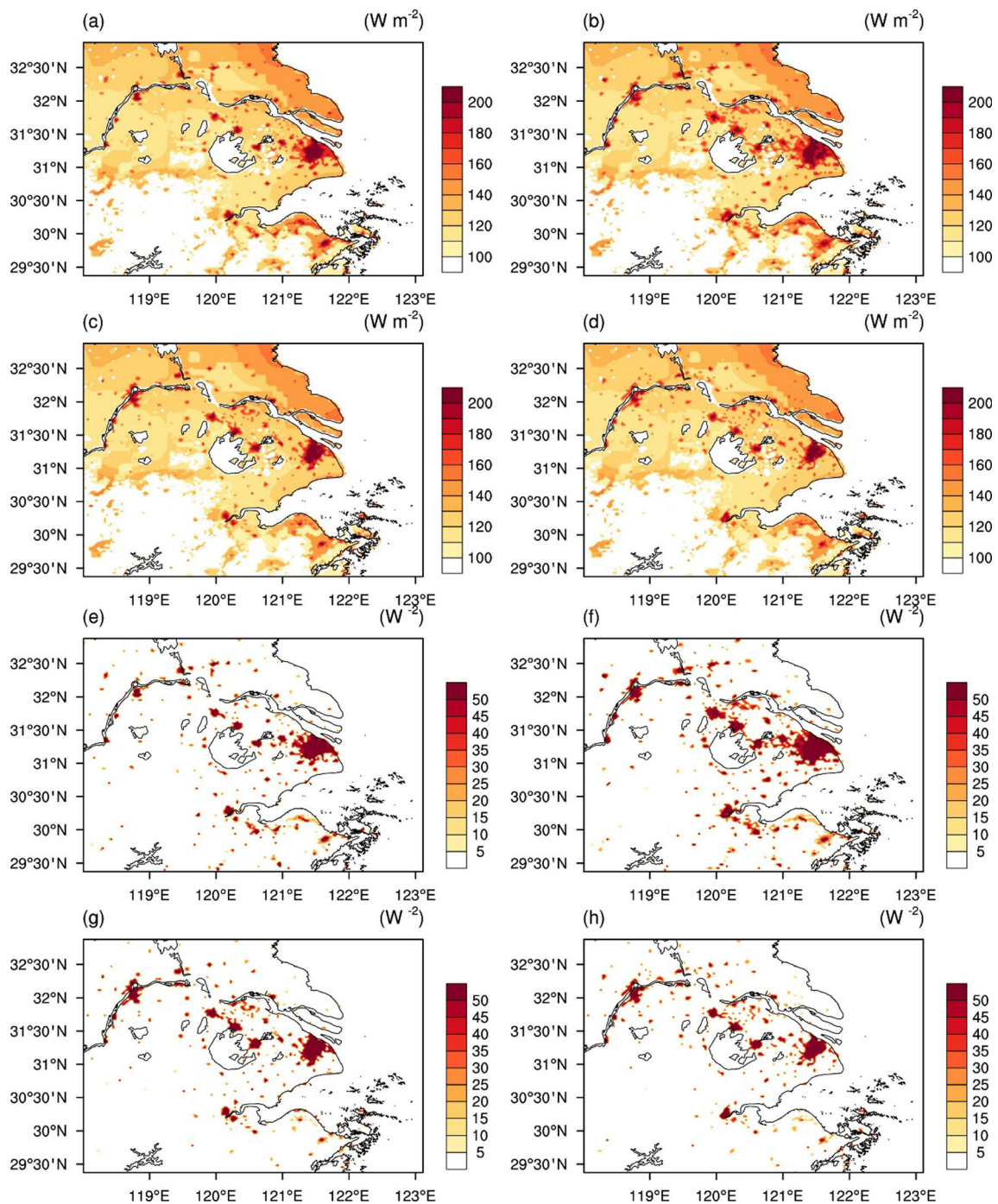


**Fig. 10** The simulated sensible heat flux in the **a** MOD, **b** CCI, **c** GLC, and **d** GLO experiments and the differences in the sensible heat flux between the MOD, **f** CCI, **g** GLC, and **h** GLO experiments and the NOURB experiment

$0.04 g kg^{-1}$ ,  $-0.02 g kg^{-1}$ , and  $-0.02 g kg^{-1}$  in the MOD, CCI, GLC, and GLO experiments, respectively, while the spatial average differences over the own-urban area were  $-0.23 g kg^{-1}$ ,  $-0.25 g kg^{-1}$ ,  $-0.23 g kg^{-1}$ , and  $-0.21 g kg^{-1}$ ; the differences over the con-urban area were  $-0.26 g kg^{-1}$ ,  $-0.31 g kg^{-1}$ ,  $-0.26 g kg^{-1}$ , and  $-0.24 g kg^{-1}$ ; and the differences over the union-urban area were  $-0.14 g kg^{-1}$ ,  $-0.21 g kg^{-1}$ ,  $-0.14 g kg^{-1}$ , and  $-0.13 g kg^{-1}$ , respectively. The

biggest change also occurred in the CCI experiments. When even the mean differences were relatively small, the EIs of near-surface-specific humidity also indicated that the urbanization have regional impact, and the values were 1.22, 1.69, 1.30, and 1.18, respectively.

More significant urban dry island occurred in the near-surface relative humidity at 2 m by the combined influence of the decrease in  $Q_{2m}$  and increase in  $T_{2m}$ . The



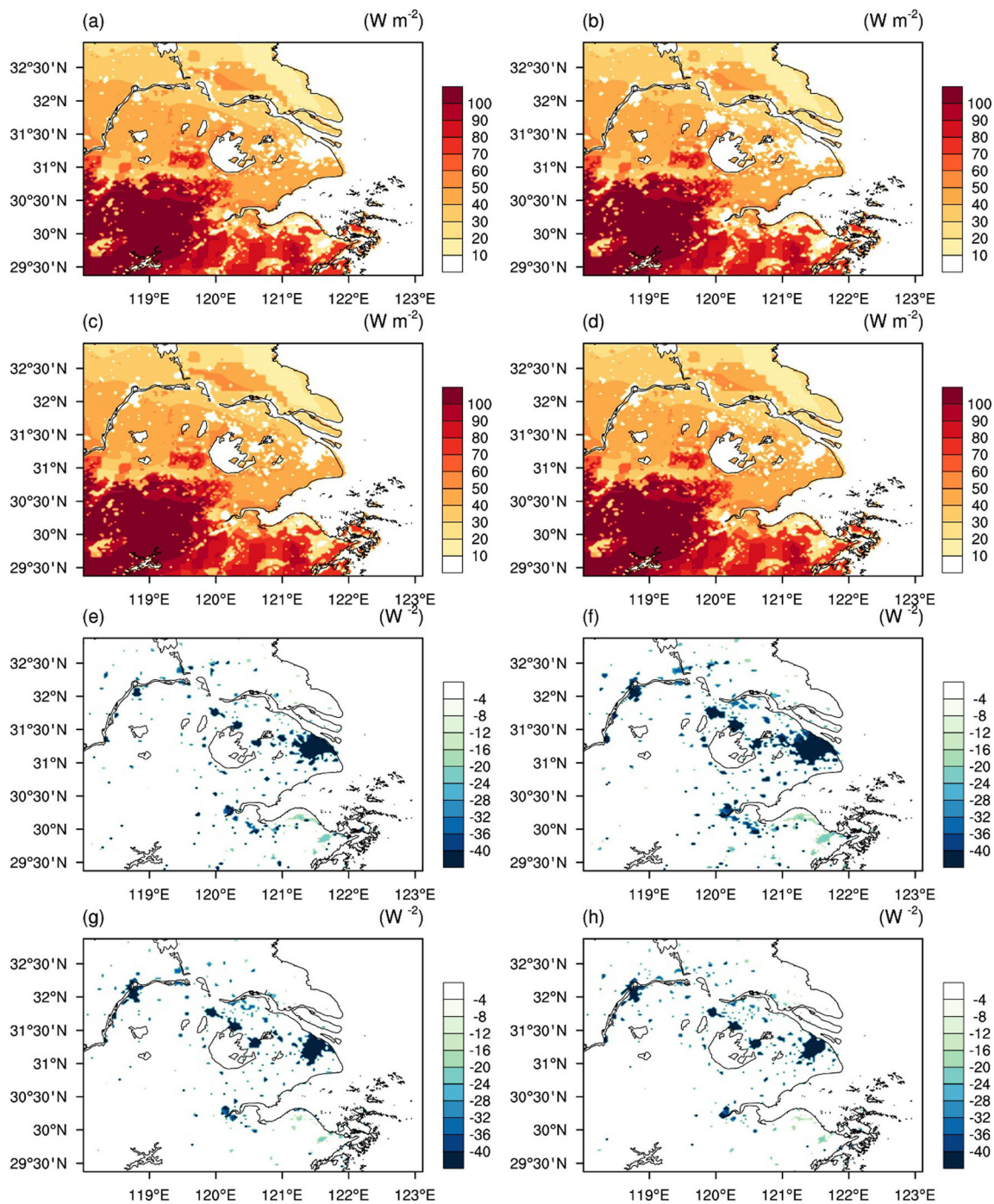


**Fig. 11** The simulated latent heat flux in the **a** MOD, **b** CCI, **c** GLC, and **d** GLO experiments and the differences in sensible heat flux between the MOD, **f** CCI, **g** GLC, and **h** GLO experiments and the NOURB experiment

mean  $RH_{2\text{ m}}$  was 53.15%, 52.91%, 53.14%, and 53.22%; the maximum was greater than 90% over the vegetation-covered grids near water bodies; and the values were 96.81%, 96.78%, 96.87%, and 96.85%. The minimum averages which occurred also over the spatial average differences in the heat episode mean surface latent heat flux were  $-0.35\%$ ,  $-0.52\%$ ,  $-0.32\%$ , and  $-0.27\%$ . The urban grid average differences were  $-2.80\%$ ,  $-3.23\%$ ,  $-3.00\%$ ,

and  $-2.64\%$  over the own-urban area;  $-3.82\%$ ,  $-4.72\%$ ,  $-3.85\%$ , and  $-3.46\%$  over the con-urban area; and  $-1.80\%$ ,  $-2.73\%$ ,  $-1.85\%$ , and  $-1.60\%$  over the union-urban area. The urbanization processes show larger EIs in the relative humidity than those in the  $Q_{2\text{ m}}$ , and the values were 1.77, 2.26, 2.25, and 1.71, because both urban warming and the loss of evapotranspiration contribute to the urban dry island in relative humidity.

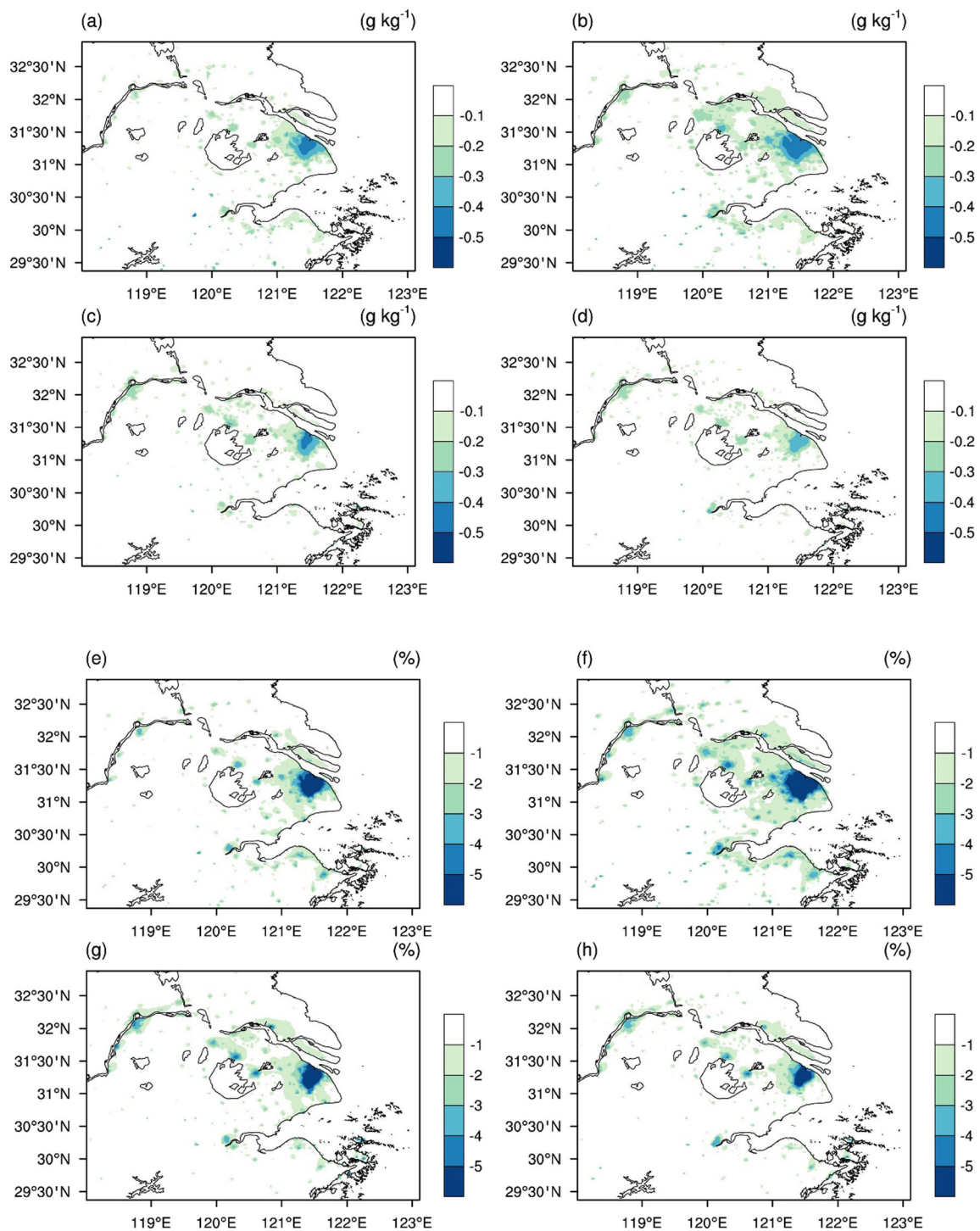


**Fig. 12** The differences in  $Q_{2m}$  between the **a** MOD, **b** CCI, **c** GLC, and **d** GLO experiments and the NOURB experiment and the differences in  $RH_{2m}$  between the **e** MOD, **f** CCI, **g** GLC, and **h** GLO experiments and the NOURB experiment

## 4 Summary and discussion

Updating the urban land cover information has been proven as a necessary step for the numerical studies of urban climate and urban atmospheric environment in such a fast urbanizing country as China. However, the urban land cover information

varies from dataset to dataset due to the raw data sources and produce methods. In this study, four sets of urban land cover information from different land cover datasets were deployed in the WRF model to investigate how the uncertainties in the input urban land use/cover (ULUC) information affect the simulations of near-surface meteorological fields, land surface

atmosphere exchanges, and heat stresses. The differences between the ULUC experiments and the NOURB experiment, in which all urban land covers were removed, were used to observe the influences of different ULUC datasets on the simulations of urbanization effects. The results show that

1. All the ULUC experiments overestimated  $T_{2\text{ m}}$  and underestimated  $Q_{2\text{ m}}$ , and this results in the underestimation of  $RH_{2\text{ m}}$ . The HI is underestimated over the rural sites and overestimated over the union-urban and con-urban sites. The ULUC experiments have some simulation skills for the  $U_{10\text{ m}}$  and  $RH_{2\text{ m}}$ . The GLO experiments output the best simulation results usually with the lowest bias and RMSE among the four ULUC experiments, especially for the  $T_{2\text{ m}}$  simulations.
2. The maximum differences in the investigated variables between the ULUC experiments and the NOURB experiment usually occur in the union-urban area, because the uncertainties among different datasets are largest in this area. Among the four ULUC experiments, the CCI experiment showed the greatest urbanization influence in all analyzed variables, because the ESA CCI dataset shows the largest urban land cover area in the analysis domain.
3. The urbanization influence on a regional climate scale is relatively little because of the low urban land cover fraction, but the urbanization influences also indicate a regional influence which means they are not limited in cities. The CCI also showed high EI values because the urban area is the largest among the ULUC experiments, but the highest EIs usually appeared in the GLC experiment, in which the urban area is the lowest. This is because the urban area distribution is more concentrated in the GLC experiment than the others, and it indicates that both city size and city shape affect the regional influence.

In the current studies, we focus only on the impact of urban land use and land cover information uncertainties on the WRF-NOAH-UCM simulations. The urban land use/land cover is also named as the external parameters (Demuzere et al. 2017), and in the future studies, more complicated factors such as the parameters of urban canopy model and anthropogenic heat release should be induced to give a full figure of the influences of the uncertainties in the description of urban land surface processes in numerical models.

**Acknowledgments** We acknowledge the Land Processes Distributed Active Archive Center (LP DAAC, <https://lpdaac.usgs.gov/>) for the MODIS data, the European Space Agency for the ESA CCI and GlobCover data, and the Food and Agriculture Organization for the GLC-SHARE data used in this study. All data are available from the corresponding author.

**Funding information** This study is supported by the Chinese National Key Research and Development Program (Grant No. 2016YFA0600303) and the National Natural Science Foundation of China (Grant No. 41675008).

**Open Access** This article is distributed under the terms of the Creative Commons Attribution 4.0 International License (<http://creativecommons.org/licenses/by/4.0/>), which permits unrestricted use, distribution, and reproduction in any medium, provided you give appropriate credit to the original author(s) and the source, provide a link to the Creative Commons license, and indicate if changes were made.

## References

- Ajaaj AA, Mishra AK, Khan AA (2017) Urban and peri-urban precipitation and air temperature trends in mega cities of the world using multiple trend analysis methods. *Theor Appl Climatol* 132:403–418. <https://doi.org/10.1007/s00704-017-2096-7>
- Amfield AJ (2003) Two decades of urban climate research: a review of turbulence, exchanges of energy and water, and the urban heat island. *Int J Climatol* 23(1):1–26
- Arsanjani JJ, Tayyebi A, Vaz E (2016) GlobeLand30 as an alternative fine-scale global land cover map: challenges, possibilities, and implications for developing countries. *Habitat International* 55:25–31
- Broxton PD, Zeng X, Sulla-Menashe D, Troch PA (2014) A global land cover climatology using MODIS data. *J Appl Meteorol Climatol* 53(6):1593–1605
- Buzan JR, Oleson K, Huber M (2015) Implementation and comparison of a suite of heat stress metrics within the Community Land Model version 4.5. *Geosci Model Dev* 8:151–170
- Chen F, Kusaka H, Bornstein R, Ching J, Grimmond CSB, Grossman-Clarke S, Loridan T, Manning KW, Martilli A, Miao S, Sailor D, Salamanca FP, Taha H, Tewari M, Wang X, Wyszogrodzki AA, Zhang CL (2011) The integrated WRF/urban modelling system: development, evaluation, and applications to urban environmental problems. *Int J Climatol* 31(2): 273–288. <https://doi.org/10.1002/Joc.2158>
- Chen Y, Zhang N (2018) Urban heat island mitigation effectiveness under extreme heat conditions in the Suzhou–Wuxi–Changzhou Metropolitan Area, China. *J Appl Meteorol Climatol* 57(2):235–253
- Demuzere M, Harshan S, Jarvi L, Roth M, Grimmond CSB, Masson V et al (2017) Impact of urban canopy models and external parameters on the modelled urban energy balance in a tropical city. *Q J R Meteorol Soc* 143(704):1581–1596
- Grimmond CSB, Blackett M, Best MJ, Baik JJ, Belcher SE, Beringer J, Bohnenstengel SI, Calmet I, Chen F, Coutts A, Dandou A, Fortuniak K, Gouvea ML, Hamdi R, Hendry M, Kanda M, Kawai T, Kawamoto Y, Kondo H, Krayenhoff ES, Lee SH, Loridan T, Martilli A, Masson V, Miao S, Oleson K, Ooka R, Pigeon G, Porson A, Ryu YH, Salamanca F, Steeneveld GJ, Tombrou M, Voogt JA, Young DT, Zhang N (2011) Initial results from phase 2 of the international urban energy balance model comparison. *Int J Climatol* 31(2):244–272
- Grimmond CSB, Blackett M, Best MJ, Barlow J, Baik JJ, Belcher SE, Bohnenstengel SI, Calmet I, Chen F, Dandou A, Fortuniak K, Gouvea ML, Hamdi R, Hendry M, Kawai T, Kawamoto Y, Kondo H, Krayenhoff ES, Lee SH, Loridan T, Martilli A, Masson V, Miao S, Oleson K, Pigeon G, Porson A, Ryu YH, Salamanca F, Shashua-Bar L, Steeneveld GJ, Tombrou M, Voogt J, Young D, Zhang N (2010) The International Urban Energy Balance Models Comparison Project: first results from phase 1. *J Appl Meteorol Climatol* 49(6):1268–1292
- Grimmond S (2007) Urbanization and global environmental change: local effects of urban warming. *Geogr J* 173(1):83–88

- Kang H-Q, Zhu B, Zhu T, Sun J-L, Ou J-J (2014) Impact of Megacity Shanghai on the urban heat-island effects over the Downstream City Kunshan. *Bound-Layer Meteorol* 152(3):411–426
- Klein P, Hu X-M, Xue M (2014) Impacts of mixing processes in nocturnal atmospheric boundary layer on urban ozone concentrations. *Bound-Layer Meteorol* 150(1):107–130
- Kusaka H, Chen F, Tewari M, Dudhia J, Gill DO, Duda MG et al (2012) Numerical simulation of urban heat island effect by the WRF model with 4-km grid increment: an inter-comparison study between the urban canopy model and slab model. *J Meteorol Soc Jpn* 90B:33–45
- Lee SH, Kim SW, Trainer M, Frost GJ, McKeen SA, Cooper OR, Flocke F, Holloway JS, Neuman JA, Ryerson T, Senff CJ, Swanson AL, Thompson AM (2011) Modeling ozone plumes observed downwind of New York City over the North Atlantic Ocean during the ICART T field campaign. *Atmos Chem Phys* 11(14):7375–7397
- Li M, Mao Z, Song Y, Liu M, Huang X (2014a) Impacts of the decadal urbanization on thermally induced circulations in Eastern China. *J Appl Meteorol Climatol* 54:259–282. <https://doi.org/10.1175/JAMC-D-14-0176.1>
- Li M, Song Y, Huang X, Li J, Mao Y, Zhu T et al (2014b) Improving mesoscale modeling using satellite-derived land surface parameters in the Pearl River Delta region, China. *J Geophys Res-Atmos* 119(11):6325–6346
- Li Y, Zhu L, Zhao X, Li S, Yan Y (2013) Urbanization impact on temperature change in China with emphasis on land cover change and human activity. *J Clim* 26(22):8765–8780
- Loveland TR, Reed BC, Brown JF, Ohlen DO, Zhu Z, Yang L, Merchant JW (2000) Development of a global land cover characteristics database and IGBP DISCover from 1 km AVHRR data. *Int J Remote Sens* 21(6–7):1303–1330
- Ma S, Pitman A, Yang J, Carouge C, Evans JP, Hart M, Green D (2018) Evaluating the effectiveness of mitigation options on heat stress for Sydney, Australia. *J Appl Meteorol Climatol* 57:209–220
- Nehrkorn T, Henderson J, Leidner M, Mountain M, Eluszkiewicz J, McKain K, Wofsy S (2013) WRF simulations of the urban circulation in the Salt Lake City area for CO<sub>2</sub> modeling. *J Appl Meteorol Climatol* 52(2):323–340
- Sherwood SC, Matthew H (2010) An adaptability limit to climate change due to heat stress. *Proc Natl Acad Sci U S A* 107:9552–9555
- Schneider A, Mertes CM (2014) Expansion and growth in Chinese cities, 1978? 2010. *Environ Res Lett* 9(2):024008
- Taha H (1997) Urban climates and heat islands: albedo, evapotranspiration, and anthropogenic heat. *Energy and Buildings* 25(2):99–103
- Taha H (2008) Urban surface modification as a potential ozone air-quality improvement strategy in California: a mesoscale modelling study. *Bound-Layer Meteorol* 127(2):219–239
- Thatcher M, Hurley P (2012) Simulating Australian urban climate in a mesoscale atmospheric numerical model. *Bound-Layer Meteorol* 142(1):149–175. <https://doi.org/10.1007/s10546-011-9663-8>
- Trusilova K, Jung M, Churkina G, Karstens U, Heimann M, Claussen M (2008) Urbanization impacts on the climate in Europe: numerical experiments by the PSU-NCAR Mesoscale Model (MM5). *J Appl Meteorol Climatol* 47(5):1442–1455
- Wang J, Yan Z, Quan X-W, Feng J (2016) Urban warming in the 2013 summer heat wave in Eastern China. *Clim Dyn* 48:1–19. <https://doi.org/10.1007/s00382-016-3248-7>
- Wang W, Zhou W, Chen D (2014) Summer high temperature extremes in Southeast China: bonding with the El Niño–Southern Oscillation and East Asian summer monsoon coupled system. *J Clim* 27(11):4122–4138. <https://doi.org/10.1175/jcli-d-13-00545.1>
- Wang X, Chen F, Wu Z, Zhang M, Tewari M, Guenther A, Wiedinmyer C (2009) Impacts of weather conditions modified by urban expansion on surface ozone: comparison between the Pearl River Delta and Yangtze River Delta regions. *Adv Atmos Sci* 26(5):962–972. <https://doi.org/10.1007/s00376-009-8001-2>
- Wang X, Liao J, Zhang J, Shen C, Chen W, Xia B, Wang T (2013) A numeric study of regional climate change induced by urban expansion in the Pearl River Delta, China. *J Appl Meteorol Climatol* 53(2):346–362. <https://doi.org/10.1175/JAMC-D-13-054.1>
- Xiao P, Wang X, Feng X, Zhang X, Yang Y (2014) Detecting China's urban expansion over the past three decades using nighttime light data. *IEEE J Sel Topics Appl Earth Observ Remote Sens* 7(10):4095–4106
- Xu R, Hu Y, Gao H, Pan Z (2017) Derivation of fractional urban signals in better capturing urbanization process. *Environ Earth Sci* 76(12):412
- Yang J, Gong P, Fu R, Zhang M, Chen J, Liang S, Xu B, Shi J, Dickinson R (2013) The role of satellite remote sensing in climate change studies. *Nat Clim Chang* 3(10):875–883. <https://doi.org/10.1038/nclimate1908>
- Yang Y, Xiao P, Feng X, Li H (2017) Accuracy assessment of seven global land cover datasets over China. *ISPRS J Photogramm Remote Sens* 125:156–173. <https://doi.org/10.1016/j.isprsjrs.2017.01.016>
- Yu M, Liu Y (2015) The possible impact of urbanization on a heavy rainfall event in Beijing. *J Geophys Res-Atmos* 120(16):8132–8143. <https://doi.org/10.1002/2015JD023336>
- Zhang D-L, Shou Y-X, Dickerson RR (2009) Upstream urbanization exacerbates urban heat island effects. *Geophys Res Lett* 36(24):L24401. <https://doi.org/10.1029/2009gl014082>
- Zhang N, Chen Y (2014) A case study of the upwind urbanization influence on the urban heat island effects along the Suzhou–Wuxi Corridor. *J Appl Meteorol Climatol* 53(2):333–345. <https://doi.org/10.1175/JAMC-D-12-0219.1>
- Zhang N, Gao Z, Wang X, Chen Y (2010) Modeling the impact of urbanization on the local and regional climate in Yangtze River Delta, China. *Theor Appl Climatol* 102(3):331–342. <https://doi.org/10.1007/s00704-010-0263-1>
- Zhang N, Wang X, Chen Y, Dai W, Wang X (2016) Numerical simulations on influence of urban land cover expansion and anthropogenic heat release on urban meteorological environment in Pearl River Delta. *Theor Appl Climatol* 126(3):469–479. <https://doi.org/10.1007/s00704-015-1601-0>
- Zhang N, Zhu LF, Zhu Y (2011) Urban heat island and boundary layer structures under hot weather synoptic conditions: a case study of Suzhou City, China. *Adv Atmos Sci* 28(4):855–865
- Zhao D, Wu J (2017) Contribution of urban surface expansion to regional warming in Beijing, China. *J Appl Meteorol Climatol* 56(6):1551–1559. <https://doi.org/10.1175/jamc-d-17-0019.1>
- Zhao L, Lee X, Smith RB, Oleson K (2014) Strong contributions of local background climate to urban heat islands. *Nature* 511(7508):216–219. <https://doi.org/10.1038/nature13462>
- Zhou L, Dickinson RE, Tian Y, Fang J, Li Q, Kaufmann RK, Tucker CJ, Myneni RB (2004) Evidence for a significant urbanization effect on climate in China. *Proc Natl Acad Sci U S A* 101(26):9540–9544
- Zhou Y, Smith SJ, Zhao K, Imhoff M, Thomson AM, Bondlamberty B et al (2015) A global map of urban extent from nightlights. *Environ Res Lett* 10(5):054011

**Publisher's note** Springer Nature remains neutral with regard to jurisdictional claims in published maps and institutional affiliations.